frontiers | Frontiers in Earth Science

TYPE Original Research
PUBLISHED 05 January 2023
DOI 10.3389/feart.2022.1016096

Check for updates

OPEN ACCESS

EDITED BY
Yefei Ren,
Institute of Engineering Mechanics, China Earthquake Administration, China

REVIEWED BY
Ying Zhou,
Jilin Jianzhu University, China
Yosuke Aoki,
The University of Tokyo, Japan

*CORRESPONDENCE
Martin Chapman,
mcc@vt.edu

SPECIALTY SECTION
This article was submitted to Structural Geology and Tectonics, a section of the journal Frontiers in Earth Science

RECEIVED 10 August 2022
ACCEPTED 21 September 2022
PUBLISHED 05 January 2023

CITATION
Guo Z and Chapman M (2023), A study of site response in the Longmen Shan and adjacent regions and site response models for the Sichuan Basin. *Front. Earth Sci.* 10:1016096. doi: 10.3389/feart.2022.1016096

COPYRIGHT
© 2023 Guo and Chapman. This is an open-access article distributed under the terms of the Creative Commons Attribution License (CC BY). The use, distribution or reproduction in other forums is permitted, provided the original author(s) and the copyright owner(s) are credited and that the original publication in this journal is cited, in accordance with accepted academic practice. No use, distribution or reproduction is permitted which does not comply with these terms.

A study of site response in the Longmen Shan and adjacent regions and site response models for the Sichuan Basin

Zhen Guo[1] and Martin Chapman[2]*

[1]School of Science, Jiangnan University, Wuxi, Jiangsu, China, [2]Department of Geosciences, Virginia Tech, Blacksburg, VA, United States

We investigated the regional attenuation and site responses in the Sichuan Basin and adjacent Songpan-Ganze terrane of the Tibetan Plateau using seismic data recorded at 41 stations from regional earthquakes occurring between January 2009 and October 2020. Fourier amplitude spectra of Lg waves were computed and binned into 18 frequency bins with center frequencies ranging from 0.1 Hz to 20.4 Hz. The quality factor is estimated as $Q(f) = 313f^{0.74}$ for the Sichuan Basin and $Q(f) = 568f^{0.34}$ for the Songpan-Ganze terrane, reflecting significant differences in the crustal structure beneath these two regions. Relative to the Songpan-Ganze terrane, site responses in the Sichuan Basin are characterized by strong amplification effects at frequencies lower than 6 Hz and obvious attenuation at higher frequencies (>10 Hz). κ_0 of stations in the Sichuan Basin show clearly geographical dependence with an average value of 0.045 s, whereas stations in the Songpan-Ganze terrane generally have smaller κ_0 values with an average value of 0.028 s. In particular, site response and κ_0 of stations in the Sichuan Basin are found to be dependent on the geographically variable thickness of the sedimentary deposits (sediment thickness). These units are comprised of sedimentary rock and semi-consolidated sediments, with a maximum thickness reaching approximately 10 km. Site response terms in the Sichuan Basin derived from the Lg Fourier spectra exhibit consistent patterns versus sediment thickness as frequency increases. We developed site response models as functions of sediment thickness for stations in the Sichuan Basin. The site response model derived from Lg site terms is consistent with that based on site response terms from coda amplitude spectra and horizontal to vertical (H/V) spectral ratios. The models were then incorporated in the stochastic method of ground motion predictions in the Sichuan Basin for six earthquakes occurring between October 2020 and June 2022. Residual analysis suggests that incorporating the site response models as functions of sediment thickness can improve the ground motion prediction model for the Sichuan Basin from moderate earthquakes.

KEYWORDS

ground motion prediction, site response, sediment thickness, Sichuan Basin, attenuation

Introduction

The Longmen Shan region is the most active seismic region in southwestern China, which has been struck by several big earthquakes since 2008, including the 12 May 2008 Ms 8.0 Wenchuan earthquake and the 20 April 2013 Ms 7.0 Lushan earthquake. The design seismic accelerations for most of the Longmen Shan and adjacent regions have been increased to 0.15–0.25 g in the latest version of seismic ground motion parameters zonation map of China issued in 2015 (AQSIQ 2001) whereas the values were 0.10–0.20 g in the previous version issued in 2001 (AQSIQ 2001). This requires that the seismic-proof demand should be raised one level or even two levels for these regions (Wang et al., 2018). Therefore, the Longmen Shan and adjacent regions, including the Sichuan Basin and Songpan-Garze Terrane (Figure 1), are currently exposed to high seismic hazard.

Ground motion prediction equations or simulations of ground motion time series play essential roles in seismic hazard analysis and other seismic engineering problems. The seismic source spectrum, path effect and site response are the three key factors in determining earthquake ground motions, where site response describes the effects of local geological conditions. It has long been recognized that near-surface geological conditions can have significant effects on earthquake ground motions. Even for rock sites, the weathering and cracking of the bedrock will amplify ground motions in certain frequency range (Steidl et al., 1996; Castro et al., 2017). For sites on unconsolidated sediments, ground motions can be strongly amplified relative to nearby rock sites whereas the high-frequency ground motions will be attenuated significantly when the sedimentary layer is thick enough (Field et al., 1997; Borcherdt 2002; Frankel et al., 2002; Wang et al., 2013; Guo and Chapman 2019; Pratt and Schleicher 2021; Wang and Wen 2021; Wang et al., 2022). Developing regional models to account for the site response effects can be challenging due to the varying geological structures beneath the seismic stations. Correction factors based on Vs. 30, which is the averaged shear-wave velocity in the top 30 m under the site, are usually adopted in ground motion prediction equations to account for the site effects (Wen et al., 2010; Bora et al., 2016; Li et al., 2018a; Stewart et al., 2020; Xu et al., 2020).

Across the Longmen Shan, the crustal thickness increases sharply from ~40 km in the western Sichuan Basin to ~60 km in the Songpan-Ganze terrane with an elevation change of ~5 km (Chen et al., 1986; Wang et al., 2007; Zheng et al., 2019; Wei et al., 2020). The Songpan-Ganze terrane is a triangular tectonic block located at the eastern margin of the Tibetan Plateau, west to the Longmen Shan thrust belt (Figure 1). This region is underlain by thick Paleozoic platform and surrounded by pre-Sinian

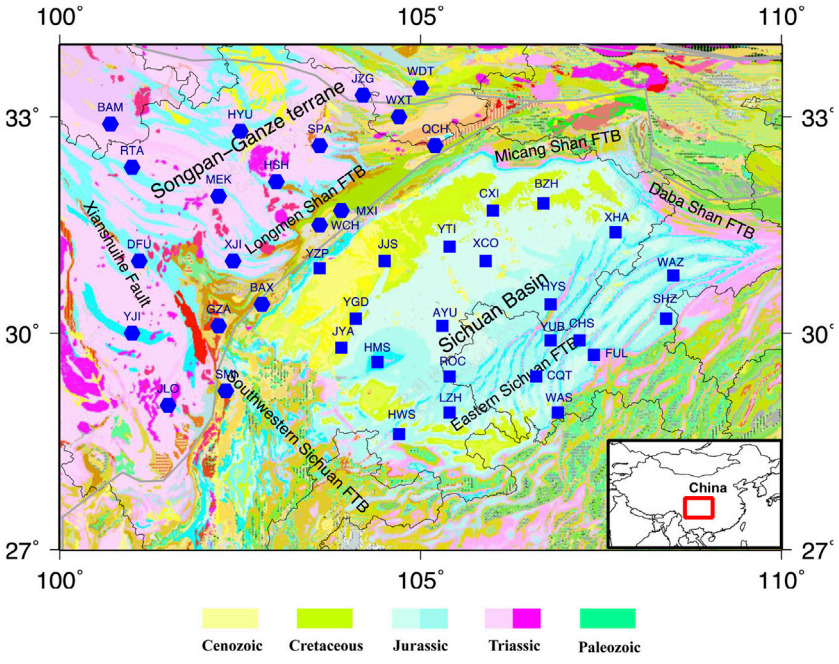

FIGURE 1
Geologic map of the Sichuan Basin and the Songpan-Ganze terrane, including the surrounding structural belts, Longmen Shan fold and thrust belt (FTB), Micang Shan FTB, Daba Shan FTB, Eastern Sichuan FTB and Southwestern Sichuan FTB. Locations of broadband stations used in this study are plotted as squares (in the Sichuan Basin) and hexagons (in the Songpan-Ganze terrane). The thick rectangle in the inset map shows the location of the study region. Geologic map is adapted from the 1:500,000 digital geological map of China, China Geological Survey (CGS, 2003).

continental basement (Zheng et al., 2016). The terrane is widely covered by Triassic marine deposits which were metamorphosed and strongly folded during late Triassic. Late Jurassic-Cenozoic sedimentary strata are lacking in this area but it does include several intrusive Miocene plutons along the deeply seated Xianshuihe fault (Chang 2000; Tian et al., 2016; Zheng et al., 2016). The Sichuan Basin is located to the east of Longmen Shan, which is a diamond-shaped compressional basin in central China and western Yangze Craton. The basin is underlain by Proterozoic rocks of the Yangtze Platform with a quite thick (up to 10 km) sedimentary cover of Mesozoic and Cenozoic marine and terrestrial sediments (Burchfiel et al., 1995; Guo et al., 1996; Meng et al., 2005; Wang et al., 2016; Xia et al., 2021). The Jurassic to Cretaceous sedimentary strata known as the "red beds," reach a thickness of ~4–6 km in the western and central basin (Guo et al., 1996; Sha et al., 2010; Li et al., 2016; Li et al., 2018b). Cenozoic sediments in the Sichuan Basin are less than 0.7 km thick and restricted to the southwestern foreland basins (Burchfiel et al., 1995; Kirby et al., 2002). The sedimentary deposits in the Sichuan Basin are characterized by wedge-shaped post-Late-Triassic strata thinning from the north and northwest towards the southeast underlain by layer-cake Early to Middle Triassic sedimentary sequences, with a total thickness varying from 2 to 10 km (Meng et al., 2005; Wang et al., 2016; Liu et al., 2021).

Previous studies have shown that the crustal quality factor, which is usually described as $Q(f) = Q_0 f^{\alpha}$, shows a smaller Q_0 but higher α in the Sichuan Basin compared to the Songpan-Ganze region suggesting different crustal structures beneath these two regions (Hua et al., 2009; Fu et al., 2018; Fu et al., 2019). Site responses in the Sichuan Basin and Songpan-Ganze region were also found to be quite different. Fu et al. (2019) studied site responses in western Sichuan Basin and the Songpan-Ganze Orogen using broadband seismograms from 88 regional earthquakes occurring between 2009 and 2013. Their results show clear differences in site responses of stations in the Sichuan Basin relative to those in the Songpan-Ganze Orogen. They also reported larger average κ_0 for stations in the western Sichuan Basin relative to the Songpan-Ganze region, coinciding with results from Fu and Li, 2016 and Li et al. (2020) using strong motion data. κ_0 here is the zero-distance kappa in Anderson and Hough (1984), which represents the attenuation effects of the near-surface geological conditions in the top hundreds of meters or even a few kilometers beneath the station. These differences in site responses are due to the various near-surface sedimentary structures in the Sichuan Basin and Songpan-Ganze terrane. Properly estimating and modeling site responses in the Longmen Shan and adjacent regions is a key step in seismic hazard analysis for southwestern China.

For regions covered by thick sediments as the Sichuan Basin, various studies have shown that the site responses are most likely controlled by the structure of the whole sedimentary column. Fu et al. (2019) found that κ_0 in the Longmen Shan region correlates apparently with the low shear-wave velocity anomaly averaged over the depth range of 0–10 km. Wang et al. (2013) studied the site responses of three stations in the Qionghai Basin to the southwest corner of the Sichuan Basin and found that site amplifications in the frequency range 0.1–10 Hz at the three stations are significantly dependent on sediment thickness in the basin. In addition, correlations between κ_0 and sediment thickness have been reported in Taiwan, the New Madrid seismic zone and the Gulf Coastal Plain (Liu et al., 1994; Campbell 2009; Chapman and Conn 2016; Chang et al., 2019). Attempts have been made to investigate and describe the correlation between the site effects and thickness of the sedimentary strata in central and eastern United States. Chapman and Conn (2016) derived a linear kappa model versus sediment thickness in the Gulf Coastal Plain and applied it into the stochastic ground motion prediction models. They showed that the kappa model significantly improved the high-frequency ground motion predictions from regional earthquakes. Following their work, Guo and Chapman (2019) investigated the site responses in the Atlantic and Gulf Coastal Plain using the spectral ratio method. They found that the site terms show obvious dependence on sediment thickness and can be modeled using piecewise linear functions versus sediment thickness at low frequencies. For the Atlantic Coastal Plain, different functions have been proposed to model the site responses with respect to sediment thickness by Harmon et al. (2019) and Pratt and Schleicher (2021) using various data sets and methods. Similar correlations between site responses and deeper sedimentary structures as well as site response models based on features of the whole sedimentary strata are expected for the Sichuan Basin.

The first objective of this paper is to compare site responses in the Songpan-Ganze terrane and Sichuan Basin due to the significantly different geological conditions. We downloaded broadband recordings from 189 regional earthquakes and computed the Fourier spectra of Lg waves which usually have the largest amplitudes in regional seismograms. Site responses and crustal attenuation were inverted simultaneously for the Sichuan Basin and Songpan-Ganze terrane respectively. The second objective of this paper is to introduce and evaluate site response models as functions of sediment thickness for the Sichuan Basin, which account for the effects of the thick sediments. In this paper, we focused on estimating the site responses and κ_0 for stations in the Sichuan Basin and Songpan-Ganze terrane using the Lg spectral amplitudes. We also obtained site response terms using coda spectral ratios and the H/V spectral ratios for stations in the Sichuan Basin, with the detailed description and comparison of the three sets of site terms of stations in the Sichuan Basin documented in a separate paper (Guo et al., 2022). The site response models for the Sichuan Basin were incorporated into the stochastic ground motion predictions for six recent earthquakes that were not included in our dataset for the inversions. The results in this paper are hoped to shed

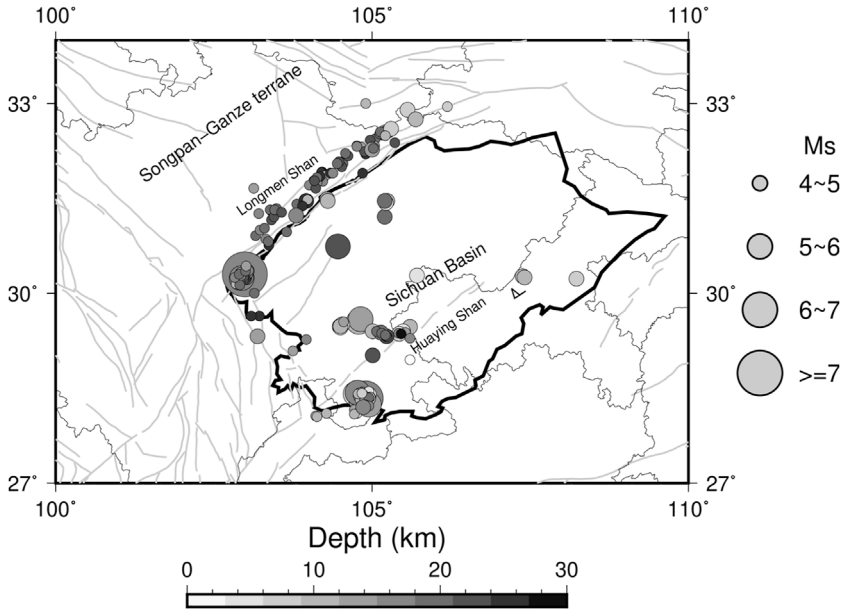

FIGURE 2
Map showing locations of the 189 earthquakes used in this study along with the earthquake source depths. Major faults in the study region are indicated by the gray lines. Magnitudes (Ms) of the earthquakes are used to scale the sizes of the circles.

light on developing regional site response models for the Longmen Shan and adjacent regions.

Data and method

Dataset

The China Digital Seismological Observation Network includes 145 broadband stations from the national seismic network and 806 broadband stations from regional seismic networks which were deployed before the end of 2007. The average spatial distance for these permanent stations is ~30–60 km except in Xinjiang and Tibet. 22 stations located in the Sichuan Basin and 19 stations in the Songpan-Ganze terrane were used in this study as shown in Figure 1. These stations have a common sample rate of 100 Hz and provide good coverage over the study region.

We collected broadband seismograms recorded at the stations from earthquakes with magnitudes $4.0 \leq Ms \leq 7.0$ happening between January 2009 and October 2020. The epicentral distances are less than 1,000 km and the focal depths are less than 30 km (Figure 2). Most of the earthquakes occurred along the Longmen Shan fault zone to the west of the Sichuan Basin and clustered in southern Sichuan Basin near the Huaying Shan fault zone as shown in Figure 2. Three-component seismograms were downloaded from the China Earthquake Network Center (CENC), beginning 2 min prior to the direct p wave with a duration of 60 min. We first obtained ground accelerations from the raw seismograms using the instrument transfer functions and rotated the two horizontal components to radial and transverse directions. The acceleration seismograms were then filtered using a high-pass filter with the corner frequency of 0.01 Hz.

To calculate the Fourier amplitude spectra of Lg waves, we adopted the following model for predicting Lg arrival time in the study region:

$$T = T_0 + \frac{r}{3.57} \quad (1)$$

where r is the epicentral distance in km and T_0 denotes the earthquake origin time. The Lg arrival time model (Eq. 1) is determined using handpicked Lg arrival times recorded at stations in the Sichuan Basin and Songpan-Ganze terrane from three earthquakes in southeastern Sichuan on 17 June, 22 June and 4 July 2019 with magnitudes Ms 5.1–5.7. The crustal velocity of Lg waves in the study region is estimated as 3.57 km/s. The length of the time window for spectral calculation is determined as 70% energy duration of the Lg waves (Chapman and Conn 2016; Guo and Chapman 2019). We tapered the time windows at both edges with 15% duration using a cosine taper and computed the Fourier amplitude spectra. Then the geometric mean of the radial and transverse Lg spectra were calculated. The noise spectra were computed simultaneously with time windows beginning at the start of the seismograms and of the same lengths as the corresponding Lg

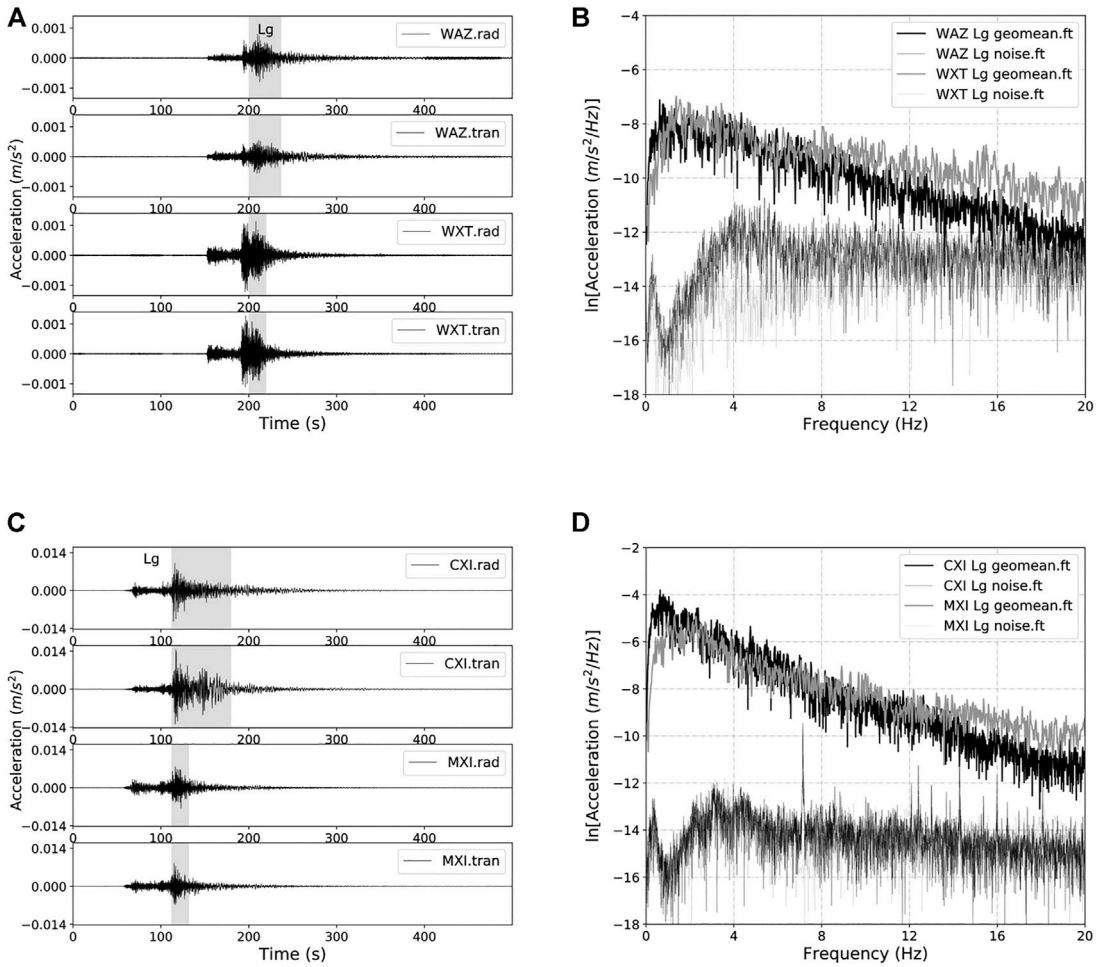

FIGURE 3
(A) Horizontal-component acceleration seismograms from the 18 December 2019 Ms 5.2 Zizhong earthquake recorded at stations WAZ (in northeastern Sichuan Basin) and WXT (in northeastern Songpan-Ganze terrane). The epicentral distances for both stations are ~374 km. The shaded areas indicate time windows used for Lg spectral calculations. **(B)** Corresponding geometric mean of Lg and noise spectra at stations WAZ and WXT. **(C)** and **(D)** are the same as **(A)** and **(B)** but from the 17 June 2019 Ms 6.0 Changning earthquake recorded at station CXI (in northwestern Sichuan Basin) and station MXI (in eastern Songpan-Ganze terrane) with epicentral distances of ~385 km.

windows. We rejected Lg spectra with signal-to-noise ratios less than three and visually inspected the spectra to exclude those with strong modulations. The final dataset consists of seismograms from 189 earthquakes with more than 5,800 event-station pairs. Supplementary Tables S1, S2 list information of the 22 stations in the Sichuan Basin and 19 stations in the Songpan Ganze terrane respectively, in which thickness of sediments beneath each individual basin station was estimated as the thickness of Cenozoic and Mesozoic sedimentary sequence from Wang et al. (2016) and Xia et al. (2021).

Figure 3 compares some examples of seismograms and Lg spectra recorded at stations in the Sichuan Basin and Songpan-Ganze terrane. In the top panel, we showed the horizontal-component seismograms and the corresponding Lg spectra recorded at station WAZ at the northeastern corner of the Sichuan Basin and station WXT in northeastern Songpan-Ganze terrane from the 18 December 2019 Ms 5.2 Zizhong, Sichuan earthquake. The acceleration amplitudes of Lg waves recorded at station WAZ are obviously smaller than station WXT though the epicentral distances are both ~374 km, corresponding to strong attenuation of Lg Fourier amplitudes relative to WXT at frequencies higher than 6–8 Hz. At lower frequencies (<1–2 Hz), we observed amplifications in Lg spectral amplitudes at station WAZ compared to WXT. Similar low-frequency amplification and high-frequency attenuation in spectral amplitudes were observed in Lg waves recorded at station CXI in northwestern Sichuan Basin and station MXI at the eastern margin of the Songpan-Ganze terrane from the 17 June 2019 Ms 6.0 Changning earthquake in southern Sichuan with epicentral distance of

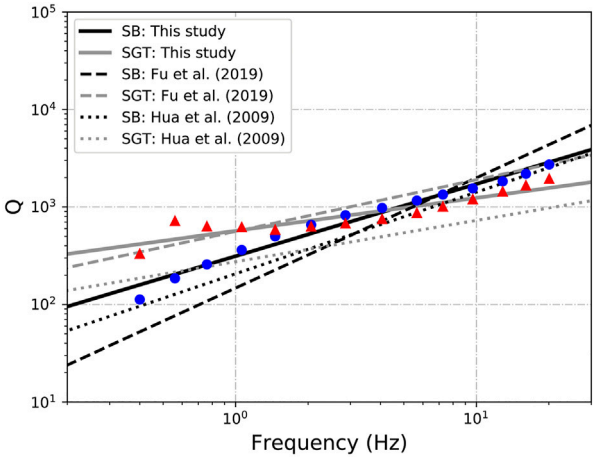

FIGURE 4
Q estimates of the Sichuan Basin (circles) and Songpan-Ganze terrane (triangles) in the frequency range of 0.4–20.04 Hz in this study. Results of least-square fits to the data are plotted as black solid line for the Sichuan Basin with $Q(f) = 335f^{0.72}$ and gray solid line for the Songpan-Ganze terrane with $Q(f) = 568f^{0.338}$ respectively. The black and gray dotted lines indicate models from Hua et al. (2009) with $Q(f) = 206.7f^{0.836}$ and $Q(f) = 274.6f^{0.423}$ for the Sichuan Basin and Songpan-Ganze terrane respectively. The black and gray dashed lines show models from Fu et al. (2019) with $Q(f) = 147.5f^{1.13}$ and $Q(f) = 274.6f^{0.53}$ for the basin and terrane respectively.

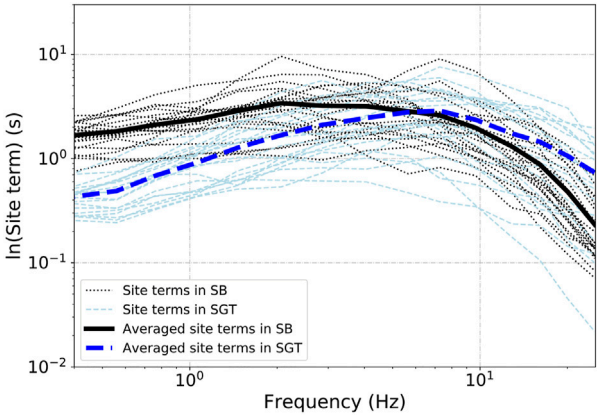

FIGURE 5
Site responses of individual stations in the Sichuan Basin (thinner dotted lines) and Songpan-Ganze terrane (thinner dashed lines) as functions of frequency. The average site response curves of stations in the Sichuan Basin and those in the Songpan-Ganze terrane are plotted as thick solid line and thick dashed line respectively.

~385 km. For further analysis, we computed the mean spectral amplitudes within 18 frequency intervals with center frequencies 0.1, 0.2, 0.3, 0.4, 0.56, 0.76, 1.06, 1.46, 2.06, 2.86, 4.06, 5.66, 7.26, 9.66, 12.86, 16.06, and 20.06 Hz respectively.

Lg spectral analysis

The spectral amplitude of Lg waves at frequency f recorded at the ith station from the kth earthquake can be modeled as the following:

$$A_{ik}(f, r_{ik}) = E_k(f)G(r_{ik})e^{-\frac{\pi r_{ik} f}{Q(f)v}}S_i(f) \quad (2)$$

where r_{ik} is the hypocentral distance, $E_k(f)$ represents the source spectrum of the kth earthquake and $G(r_{ik})$ is the geometrical spreading term. V is the shear-wave velocity and $Q(f)$ is the quality factor in the crust. The site response term at ith station is denoted as $S_i(f)$.

Our goal is to invert for the crustal quality factor $Q(f)$ and site response term $S_i(f)$ for sites in the Sichuan Basin and Songpan-Ganze terrane, which requires appropriate modeling of the source term and geometrical spreading effect according to Eq. 2. Here we modeled the source spectrum of kth earthquake using an omega-square source model, the Brune source spectral model (Brune, 1970, 1971), as the following equation:

$$E_k(f) = R_{\theta\phi}F_S V \frac{M_0(2\pi f)^2}{1 + \left(\frac{f}{f_c}\right)^2} \frac{1}{4\pi\rho\beta^3} \quad (3)$$

in which $R_{\theta\phi} = 0.55$ is the radiation pattern averaged over a proper range of take-off angles and azimuths, $F_S = 2$ represents the free-surface effect and V accounts for the partition of S-wave energy into the horizontal components set to 0.71. ρ and β are density and shear-wave velocity near the source, assumed to be 2.7 g/cm^3 and 3.57 × 10^5 cm/s respectively. M_0 is the earthquake seismic moment. The corner frequency $f_c = 0.491\beta\left(\frac{\Delta\sigma}{M_0}\right)^{\frac{1}{3}}$, in which M_0 is in units of dyn·cm, $\beta$is in units of cm/s and $\Delta\sigma$ denotes the earthquake stress drop in units of dyn/cm^2. Here we adopted a stress drop value of 1 MPa according to the results from Fu et al. (2018), Wang et al. (2018) and Li et al. (2020) for earthquakes occurring along the Longmen Shan fault zone and clustered in the southern Sichuan Basin.

Geometrical spreading of S and Lg waves at near-source distances is known to be complex due to the effects of radiation pattern, focal depth, source directivity and postcritical reflections from the Moho and intra-crustal velocity contrasts (Burger et al., 1987; Ou and Herrmann 1990; Atkinson and Mereu 1992; Atkinson and Boore, 2014). At larger distances, the Lg geometrical spreading can be simply modeled as $G(r_{ik}) = r_{ik}^{-0.5}$ (Kennett 1986). We used trilinear models similar to those of Atkinson and Mereu (1992) to account for the geometrical spreading effects in the Sichuan Basin and Songpan-Ganze terrane:

TABLE 1 Kappa (κ_0) estimates from Lg Fourier spectral amplitudes of stations in the Sichuan Basin and Songpan-Ganze terrane.

Station (sichuan Basin)	κ_0 (s)	Station (songpan-ganze terrane)	κ_0 (s)
YZP	0.047	SPA	0.03
CHS	0.059	HYU	0.057
CQT	0.046	HSH	0.035
FUL	0.041	MEK	0.023
ROC	0.058	XJI	0.022
SHZ	0.034	BAM	0.022
WAZ	0.046	RTA	0.033
YUB	0.022	DFU	0.064
AYU	0.06	YJI	0.023
BZH	0.052	JLO	0.038
CXI	0.071	BAX	0.025
HMS	0.027	GZA	0.024
HWS	0.04	SMI	0.029
HYS	0.025	JZG	0.013
JJS	0.081	WDT	0.024
JYA	0.05	WXT	0.011
LZH	0.038	QCH	0.022
XCO	0.056	MXI	0.017
XHA	0.03	WCH	0.028
YGD	0.051		
YTI	0.044		
WAS	0.022		

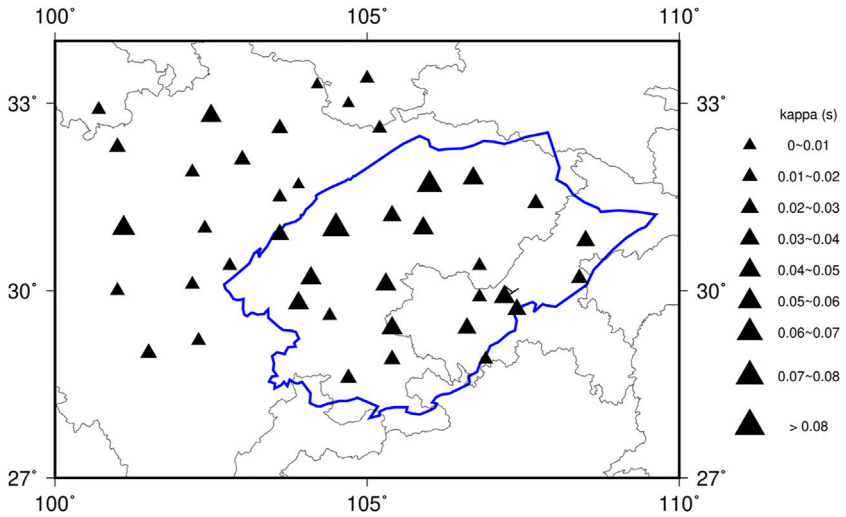

FIGURE 6
κ_0 of stations in the Sichuan Basin and Songpan-Ganze terrane plotted at the geographical locations of the corresponding stations. Sizes of the triangles are scaled to the values of κ_0 in seconds. The margin of the Sichuan Basin is shown by the thick line.

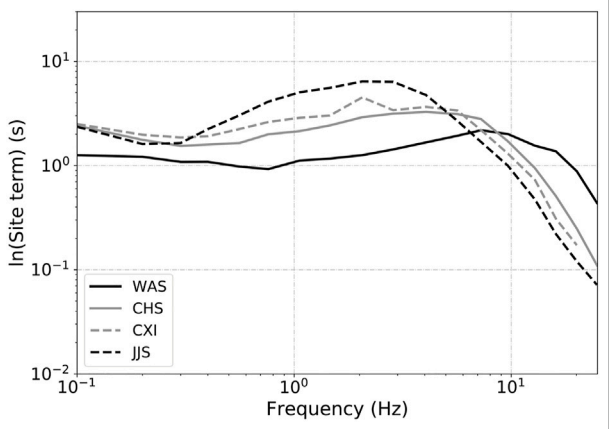

FIGURE 7
Comparison of site responses versus frequency of four stations WAS, CHS, CXI, and JJS in the Sichuan Basin. The thicknesses of sediments underlying stations WAS, CHS, CXI, and JJS are 2.0, 5.2, 7.7 and 10.0 km respectively. The value of sediment thickness is estimated as the thickness of the Cenozoic and Mesozoic sedimentary sequence based on results from Wu et al. (2016).

TABLE 2 Linear regression coefficients of natural logarithms of Lg site terms and all three sets of site terms as a function of sediment thickness in km at each center frequency (*f*).

f (Hz)	Lg site term		All site term	
	a	b	*a*	b
0.1	0.0648	0.3456	0.0623	0.1742
0.56	0.0866	0.0816	0.0621	0.0550
0.76	0.1136	0.0698	0.0892	0.0373
1.06	0.1150	0.1874	0.0893	0.1564
2.06	0.1359	0.3654	0.1111	0.2121
4.06	0.1304	0.3594	0.1104	0.0599
5.66	0.0825	0.4946	0.0780	0.0795
7.26	0.0055	0.7808	-0.0013	0.3793

$$G(r_{ik}) = \begin{cases} r_{ik}^{-1.0}, & r_{ik} \le 1.5\,H \\ (1.5H)^{-1.0}, & 1.5H < r_{ik} < 2.5\,H \\ (1.5H)^{-1.0}\left(\dfrac{r_{ik}}{2.5H}\right)^{-0.5}, & r_{ik} \ge 2.5\,H \end{cases} \quad (4)$$

where H is the Moho depth. Here we took H = 42 km for the Sichuan Basin and H = 60km for the Songpan-Ganze terrane according to results in Wang et al. (2007), Li et al. (2011) and Wei et al. (2020).

For inversion, we wrote Eq. 2 as the following:

$$\ln\left[\frac{A_{ik}(f, r_{ik})}{E_k(f)G(r_{ik})}\right] = -\frac{\pi f r_{ik}}{Q(f)v} + \ln[S_i(f)] \quad (5)$$

The quality factor $Q(f)$ and site term $S_i(f)$ at each centered frequency f can be estimated from the linear regression of Eq. 5 with respect to hypocentral distance r_{ik}. All the 189 earthquakes were used in the inversion for the Sichuan Basin while we only used seismic data from 149 earthquakes along the Longmen Shan fault zone in the inversion for the Songpan-Ganze terrane to ensure that most of the propagation paths are within the terrane. The site terms for *ith* station at high frequencies can be modeled as the following:

$$\ln[S_i(f)] = \ln[C_i] - \pi\kappa_i f \quad (6)$$

where C_i is a constant and κ_i is the zero-distance kappa (κ_0) at the *ith* station. We then estimated κ_i from a linear regression of Eq. 6 with respect to frequency. The frequency range of the linear regression is constrained by the signal-to-noise ratios and the linear trend of the natural logarithms of the site terms.

Results

Q in the Sichuan Basin and Songpan-Ganze terrane

The Lg wave is typically the most prominent phase in seismograms at regional distances over continental paths. The Lg attenuation in the crustal wave guide was found to be sensitive to the lateral changes in crustal structure, intrinsic properties and deformation of the crust (Frankel 1991; Baqer and Mitchell 1998; Xie et al., 2006; Pasyanos et al., 2009; Zhao et al., 2010). Figure 4 shows the quality factor Q inverted from Eq. 5 for the Sichuan Basin and Songpan-Ganze terrane. The Q values in both regions generally increase with frequency. At frequencies higher than 2 Hz, both sets of Q exhibit good linear trends versus frequency in log-log scale and the quality factor in the basin is larger than that in the Songpan-Ganze terrane, suggesting less attenuation of high frequency motion through the basin crust. The least square fits to the Q values are plotted as solid lines in Figure 4, corresponding to the following models:

$$Q(f) = 313 f^{0.74} \quad (7)$$

for the Sichuan Basin, and

$$Q(f) = 568 f^{0.34} \quad (8)$$

for the Songpan-Ganze terrane. Q models for these two regions from Fu et al. (2019) and Hua et al. (2009) were also plotted in Figure 4. In general, Q models in the three studies all show larger low-frequency Q and smaller high-frequency Q in the Songpan-Ganze region relative to the Sichuan Basin. The Q models in this study have larger Q_0 (Q at 1Hz) values and smaller slopes compared to previous studies, for both regions. $Q(f)$ for the Songpan-Ganze terrane from Hua et al. (2009) predicted obviously smaller values than the other two models. Discrepancies in Q models among the three studies are

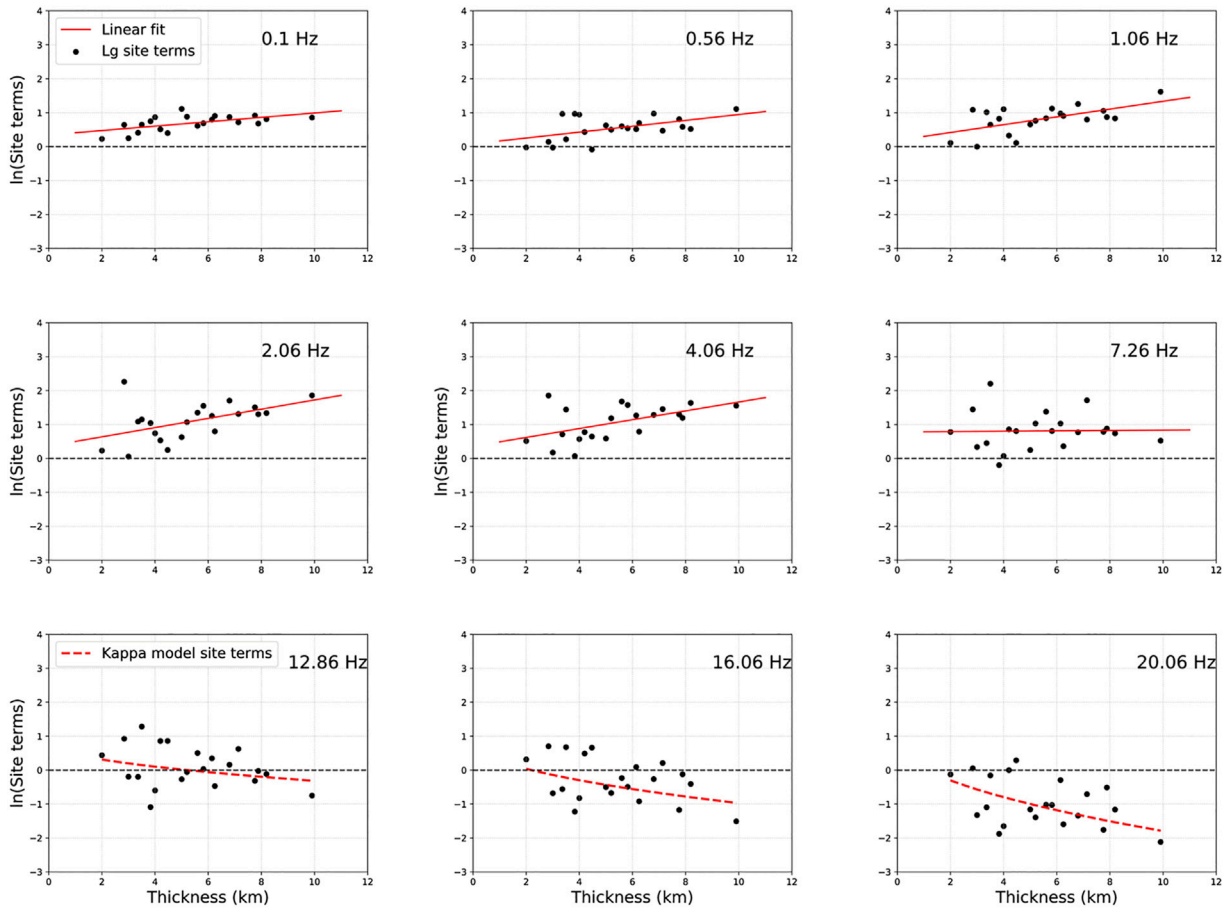

FIGURE 8
Natural logarithms of site terms (dots) estimated from linear regression of Eq. 8 using Lg waves for stations in the Sichuan Basin versus sediment thickness over frequency range 0.1–7.26 Hz. The solid lines indicate linear regression results of the Lg site terms with respect to sediment thickness. The dashed lines show estimates calculated using Eq. 6 and the κ_0 model represented by Eq. 10.

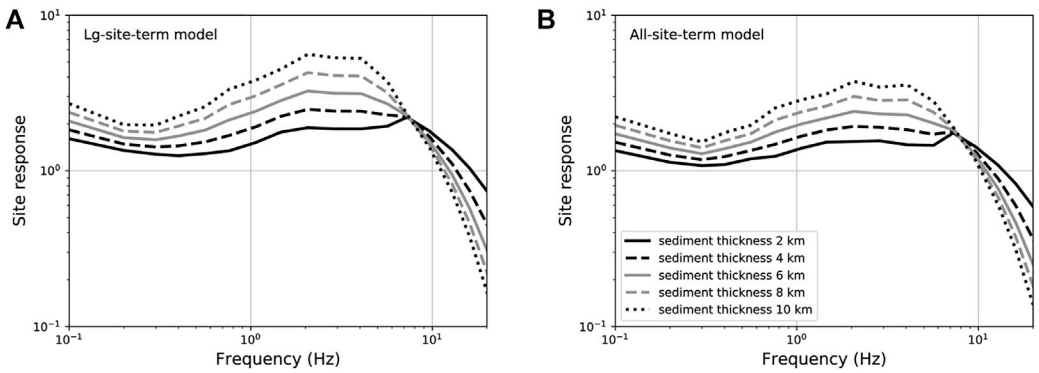

FIGURE 9
Site responses calculated using Eqs 9, 11 for sites in the Sichuan Basin with different sediment thicknesses.

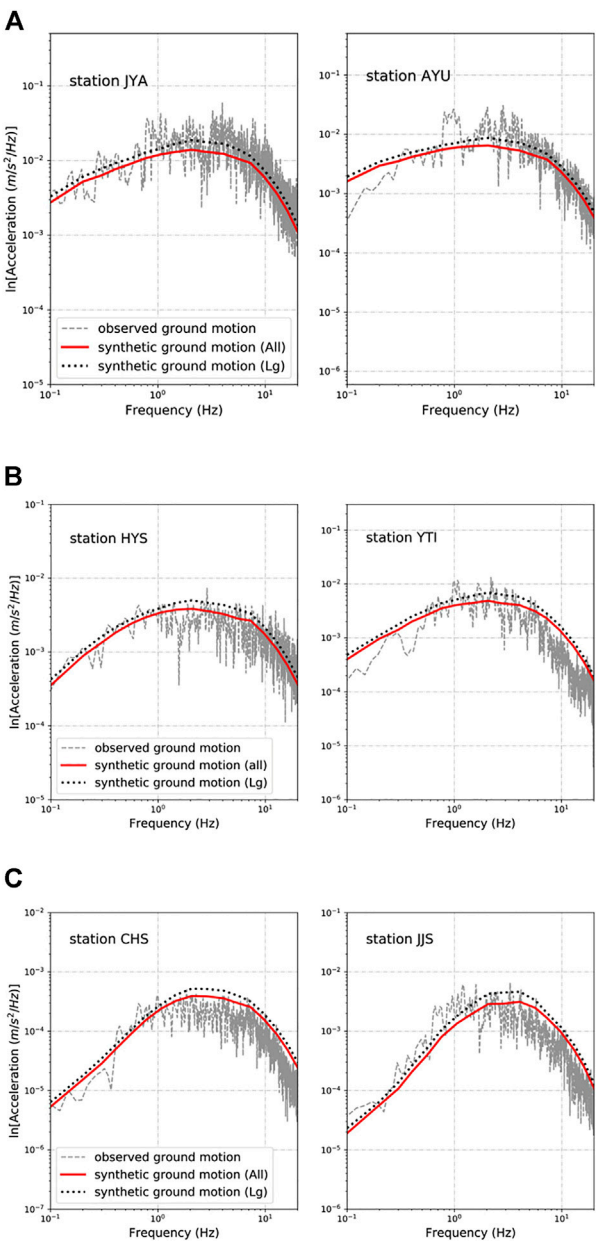

FIGURE 10
(A) The gray dashed lines show the Lg spectra recorded at stations JYA and AYU in the Sichuan Basin from the 1 June 2022 Ms 6.1 Lushan earthquake respectively. The dotted and solid lines indicate the corresponding target spectra calculated using Eq. 2 based on site response terms with Lg site term coefficients and all site term coefficients listed in Table 2 respectively. **(B)** The same as **(A)** but for Lg waves recorded at stations HYS and YTI in the Sichuan Basin from the 15 September 2021 Ms 6.0 earthquake. **(C)** The same as **(A)** and **(B)** but for Lg waves recorded at stations CHS and JJS in the Sichuan Basin from the 21 October 2020 Ms 4.6 earthquake in central Sichuan.

attributed to the different dataset, methods and study area covered by the ray paths. At high frequencies (f > 4 Hz), larger Q values in the Sichuan Basin may indicate less heterogeneities in the deep crust beneath the basin sedimentary sequence. It is important to note that, from Eq. 2, the Q estimates above reflect the distance dependent part of the total attenuation through the path, and presumably quantify Q in the deeper crust. Distance independent attenuation occurring essentially beneath the receivers (zero distance) and presumably at shallower depths is captured by the $S_i(f)$ site terms in Eq. 2. The total path attenuation (the product of both the exponential and site terms on the right-hand side of Eq. 2) at most sites in the Sichuan Basin at high frequencies (f > 4 Hz) is actually greater than at most sites in the Songpan-Ganze terrane. Attenuation occurring along the part of the path essentially beneath the receivers is quantified by larger average values of κ_0 in the Sichuan Basin compared to the Songman-Ganze terrane. We discuss this complex behavior of site response in the following sections.

Site responses in the Sichuan Basin and Songpan-Ganze terrane

In Figure 5, we showed the site response terms of stations in the Sichuan Basin and Songpan-Ganze terrane. Site responses for most of the stations exhibit a wide frequency range of amplification instead of a distinguishable resonant peak and site responses in the Sichuan Basin are significantly different from those in the Songpan-Ganze terrane. The peak amplifications for sites in the Sichuan Basin mainly occur between 1 and 4 Hz, whereas they exist between 2 and 11 Hz for stations in the Songpan-Ganze terrane. This can be clearly observed in the average site response curves for the two regions shown in Figure 5. The average site response in the Sichuan Basin indicates strong amplifications over the frequency range up to ~15 Hz while stations in the Songpan-Ganze terrane tend to amplify ground motions in the frequency range of 1.7–18 Hz. At frequencies lower than 1.7 Hz, average de-amplifications are observed for the Songpan-Ganze stations. The average site response in the Sichuan Basin shows much stronger amplification at low frequencies (<6 Hz) and more obvious attenuation at frequencies higher than 10 Hz relative to the Songpan-Ganze terrane. The average peak frequency for sites in the Sichuan Basin is ~2 Hz with an amplification factor of ~3.3 while it migrates to ~7 Hz with a peak factor of ~2.4 in the Songpan-Ganze terrane. For individual sites, the peak amplification factor could reach up to ~10 in the Sichuan Basin. Fu et al. (2019) calculated site responses for 16 stations

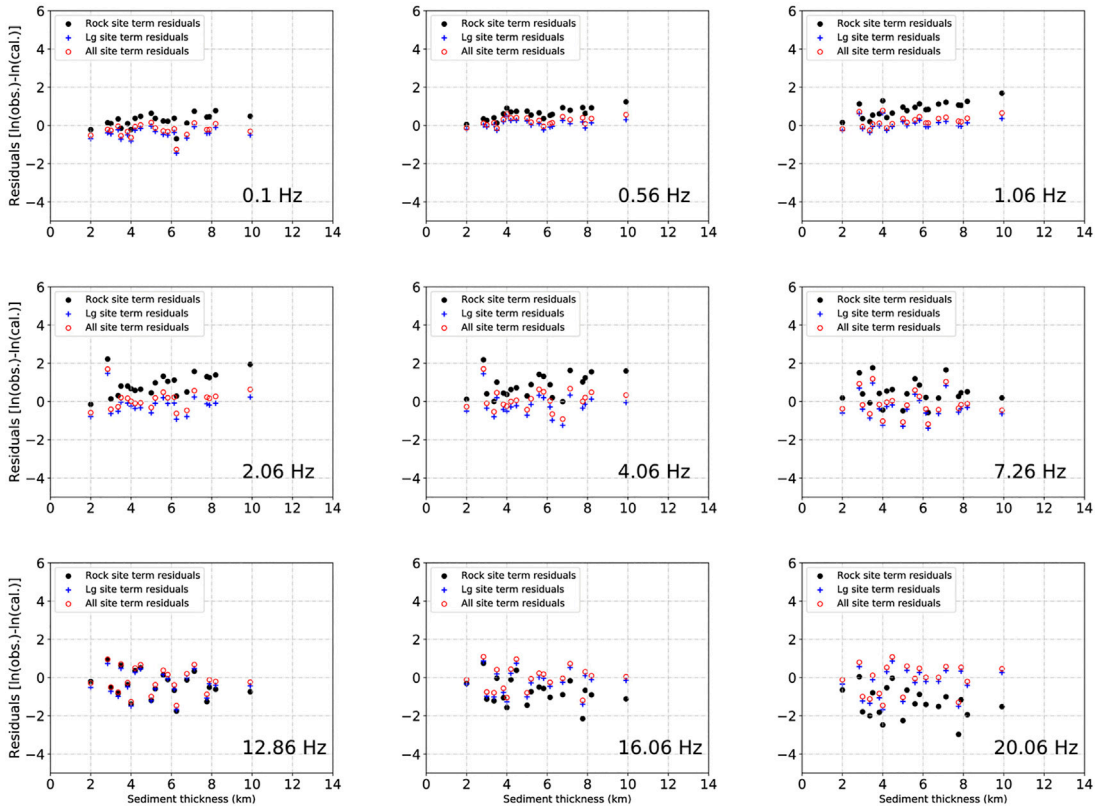

FIGURE 11
Rock site term residuals (filled circles), Lg site term residuals (pluses) and all site term residuals (open circles) of stations in the Sichuan Basin at different frequencies plotted with respect to sediment thickness in the basin for the 1 June 2022 Ms 6.1 Lushan earthquake.

in western Sichuan Basin and 12 stations in eastern Songpan-Ganze terrane using the generalized inversion technique (GIT). Their results are similar to the site responses in our Figure 5.

Table 1 lists the estimates of κ_0 from Lg Fourier spectra for the stations in the Sichuan Basin and Songpan-Ganze terrane which were plotted at the geographical locations of the corresponding stations in Figure 6. The largest κ_0 values occur in western and central Sichuan Basin while κ_0 of stations in eastern Sichuan Basin and the Songpan-Ganze terrane are generally smaller. κ_0 values in the Songpan-Ganze terrane are within 0.011–0.038 s except for stations DFU and HYU with κ_0 values of 0.064 s and 0.057 s respectively, whereas κ_0 varies significantly from 0.02 s to 0.08 s across the Sichuan Basin. The average κ_0 in the Sichuan Basin is 0.045 s, larger than the average κ_0 in the Songpan-Ganze terrane with a value of 0.028 s. Fu et al. (2019) obtained similar results with average κ_0 values of 0.0423 s and 0.0227 s for western Sichuan Basin and the Songpan-Ganze Orogen respectively using the GIT. The stronger high-frequency attenuation effects implied by the larger κ_0 values in the Sichuan Basin relative to the Songpan-Ganze terrane are likely due to the thick unconsolidated and semi-consolidated Post-Triassic sediments accumulated in the basin. Geographical variation of κ_0 in the Sichuan Basin is significant and it is notable that the κ_0 generally decreases from northwest towards southeast within the basin coinciding with the changes of sediment thickness (Meng et al., 2005; Wang et al., 2016; Li et al., 2020).

Site response models for the Sichuan Basin

The Sichuan Basin is the most populated and industrialized area in southwestern China, and therefore exposed to higher seismic hazard than adjacent regions near the Longmen Shan fold and thrust belt. Developing appropriate ground motion prediction models for the Sichuan Basin is in urgent demand for seismic hazard analysis, which will require an appropriate site response model to account for the amplification and attenuation effects of the thick sediments in the basin.

Figure 7 shows site response terms versus frequency for four stations in the Sichuan Basin underlain by sedimentary columns of different thicknesses. As the sediment thickness increases, the peak frequency of amplifications generally migrates to lower

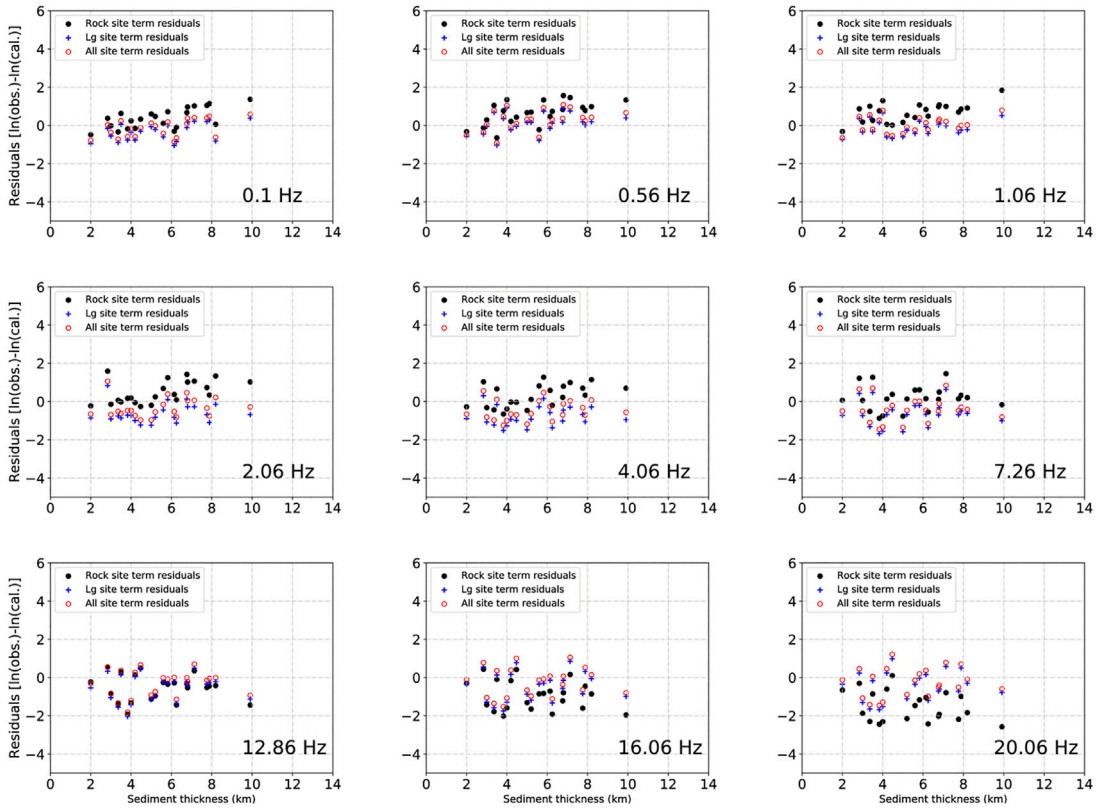

FIGURE 12
Same as Figure 11 but for the 21 October 2020 Ms 4.6 earthquake in central Sichuan.

frequencies and the amplitudes of amplifications become larger. At high frequencies (>10 Hz), we observed stronger attenuation effects at stations overlying thicker sediments. These observations imply that site responses in the Sichuan Basin are strongly correlated with sediment thickness.

In Figure 8, we plotted the natural logarithms of the site terms derived from Lg Fourier spectra with respect to sediment thickness at nine center frequencies ranging from 0.1 to 20.06 Hz. Some patterns can be observed, even though the scatter is large. At lower frequencies ($\leq$ 4.06 Hz), the site responses were dominated by amplifications and exhibit positive correlations with sediment thickness. As frequency increases, the positive trend becomes flat and gradually turns into a negative trend within the frequency range of 7–12 Hz. The site responses show dominant attenuations at frequencies higher than 12.86 Hz and the attenuation effects become more significant as sediment thickness increases. To verify the sediment-thickness dependence of the site response terms, we also calculated site responses in the Sichuan Basin using the H/V spectral ratios and coda spectral ratios. The results show that site response terms derived from the three different methods behave consistently versus sediment thickness as frequency increases. Detailed description of the three sets of site response terms has been documented in a separate paper (Guo et al., 2022).

We model the site responses at frequency f in the Sichuan Basin using the following linear relationship between the natural logarithm of the site terms and sediment thickness:

$$\ln[S(f,Z)] = aZ + b \tag{9}$$

where Z is sediment thickness in km. Eq. 9 is only used to model the site responses within the frequency range of 0.1–7.26 Hz and the linear regression results are plotted as solid lines in Figure 8. At higher frequencies, the site responses are controlled by κ_0 according to Eq. 6. κ_0 values of stations in the Sichuan Basin derived from Lg spectral amplitudes agreed well with those from the coda spectral ratios as shown in Supplementary Figure S1 (Supplementary Materials), and both sets of κ_0 exhibit a clear positive correlation with sediment thickness. κ_0 estimates from Fu et al. (2019) are also within the scatter range of our κ_0 values. We modeled κ_0 in the Sichuan Basin as a function of sediment thickness following Guo and Chapman (2019):

$$\kappa_0 = 0.019Z^{0.545} \tag{10}$$

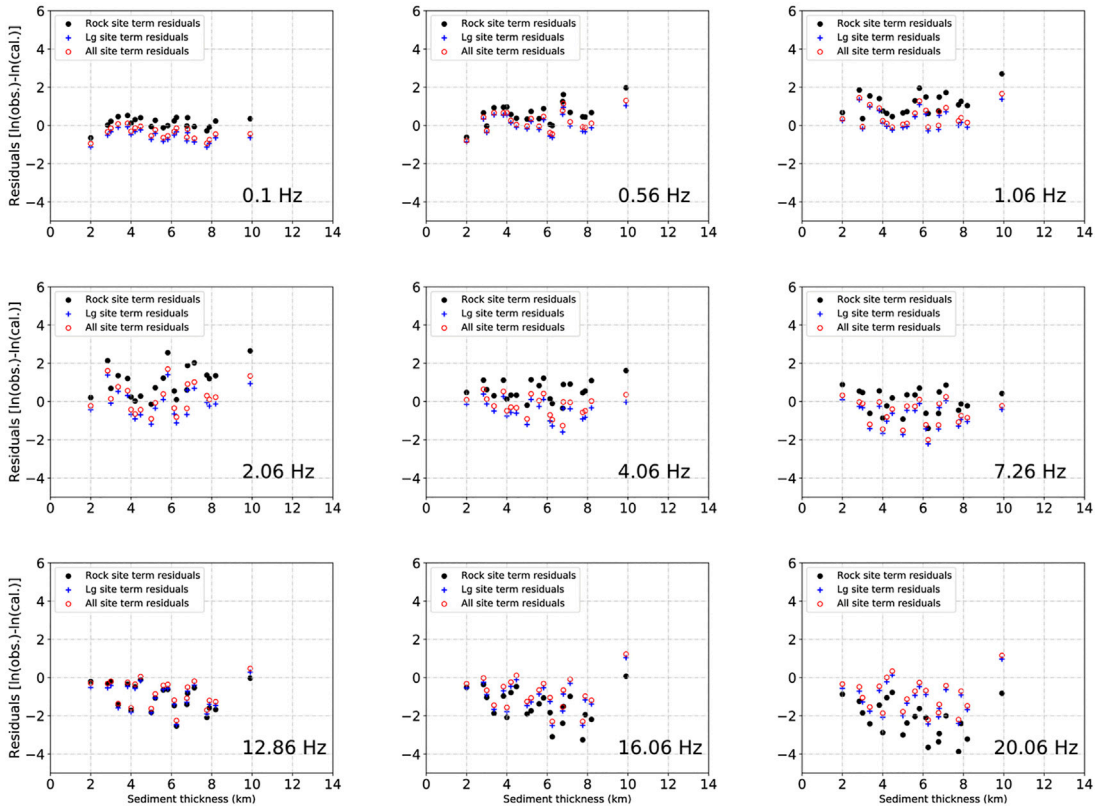

FIGURE 13
Same as Figure 11 but for the 15 September 2021 Ms 6.0 earthquake.

Here the units for κ_0 and sediment thickness are seconds and kilometers respectively. For frequencies higher than 7.26 Hz, the site responses are modeled as the following:

$$\ln[S(f,Z)] = \ln[S(7.26\,Hz,Z)]e^{-\pi\kappa_0(f-7.26)} \quad (11)$$

where κ_0 is defined by Eq. 10 as a function of sediment thickness. As shown by the dashed lines in Figure 8, the model represented by Eq. 11 fits the observed Lg site terms well.

Table 2 lists the coefficients for linear regressions of the Lg site terms in the frequency range of 0.1–7.26 Hz. For comparison, we also listed the linear regression coefficients of all site response terms estimated from the three different methods in Table 2. Figure 9 shows some examples of site response models $S(f,Z)$ versus frequency for the Sichuan Basin. Site response curves for sediment thickness ranging from 2 to 10 km in Figure 9A were calculated using the Lg site term coefficients while those in Figure 9B were calculated using the all site term coefficients. The Lg site term model is similar to the corresponding all site term model but has slightly larger amplitudes.

Evaluation of the site response models

To evaluate the site response models defined by Eqs 9, 11 as functions of frequency and sediment thickness, we applied the models using the stochastic method of ground motion simulation for the Sichuan Basin following Guo and Chapman (2019). We selected six earthquakes occurring between October 2020 and June 2022 with magnitude (Ms) of 4.6–6.1 for analysis. Seismograms from these earthquakes were not included in the dataset for estimating the quality factor and site response: therefore, they can be used for an unbiased test of our attenuation and site response model. Detailed information for the six earthquakes was listed in Supplementary Table S3. Three of the earthquakes were located along the western boundary of the Sichuan Basin and the rest of them occurred in the southern part of the basin.

We first calculated the synthetic Fourier amplitude spectrum (i.e., target spectrum) for each station-event pair using Eq. 2 based on the stochastic method. The source and geometrical spreading terms are given by Eqs 3, 4, and the quality factor $Q(f)$ in the Sichuan Basin is modeled as Eq. 7. The site response term is

defined by Eqs 9, 11. Figure 10 shows examples of observed and target spectra from three of the earthquakes in Supplementary Table S3. In Figure 10A, we showed the target spectra for stations JYA and AYU from the 1 June 2022 Ms 6.1 Lushan earthquake calculated using the site response models based on the Lg site term and all site term coefficients listed in Table 2 respectively. The target spectrum based on Lg site term coefficients has slightly higher amplitudes than that based on all of the site term coefficients. In general, the shape and amplitudes of the observed Lg spectra have been well-captured by both target spectra.

For further investigation, we computed three sets of residuals which are differences between the observed and target spectra for each station-event pair. Two sets of the residuals were calculated using target spectra based on site response models defined in Eqs 9, 11 with Lg site term and all site term coefficients respectively. We denoted these two sets of residuals as "Lg site term residuals" and "all site term residuals" hereafter. The third set of residuals were calculated using the site response term for generic rock sites defined as the following equation:

$$S_r(f) = C_r e^{-\pi \kappa_r f} \tag{12}$$

in which C_r is the crustal amplification factor from Boore and Thompson (2015) for rock sites with a V_{S30}=2.0 km/s, and κ_r = 0.006 *s* which is representative of hard rock sites. We denoted the third set of residuals as "rock site term residuals".

Figure 11 shows the three sets of residuals versus sediment thickness at nine frequencies for the 1 June 2022 Ms 6.1 Lushan earthquake, which occurred near the southwestern corner of the Sichuan Basin. The rock site term residuals show a strong frequency dependence with positive amplitudes at frequencies lower than 4.06 Hz while the amplitudes decrease to negative values at higher frequencies ($\geq$ 12.84 Hz). Sediment thickness dependence was clearly observed in the rock site term residuals. The amplitudes of the residuals become more positive for sites on larger thicknesses of sediment at frequencies lower than 4.06 Hz whereas they decrease to more negative values as thickness increases at higher frequencies ($\geq$ 12.84 Hz). The Lg site term and all site term residuals behaved consistently with each other and showed minor differences over the frequency range. Relative to the rock site term residuals, the Lg and all site term residuals exhibit a lack of thickness dependence and the amplitudes are brought down to near zero at frequencies ranging from 0.56 to 4.06 Hz and increase to near zero at frequencies higher than 12.86 Hz. Similar reductions in residual bias when using the site response models derived in this study were observed in residuals for the 21 October 2020 Ms 4.6 earthquake in central Sichuan and the 15 September 2021 Ms 6.0 earthquake in southern Sichuan Basin as shown in Figures 12, 13. For the Ms 6.0 earthquake in the southern Sichuan Basin, the ground motion prediction models with Lg and all site term coefficients tend to overestimate the ground motions at high frequencies ($\geq$ 12.86 Hz). However, the thickness dependence in the rock site term residuals is absent in the Lg and all site term residuals and the site response models with Lg and all site term coefficients greatly improved the prediction of high-frequency ground motions relative to that with the rock site term. Supplementary Figure S2 shows residuals for the remaining three earthquakes in Supplementary Table S3 which share similar behaviors with the residuals in Figures 11–13. At certain frequency range (especially 4.06–7.26 Hz), the average values of the Lg and all site term residuals for the six earthquakes deviated from zero suggesting the site response models defined by Eqs 9, 11 are not working well for these frequencies. However, the ground motion prediction models with Lg and all site term coefficients generally worked better in predicting ground motions in the Sichuan Basin for the six earthquakes relative to the prediction model using the rock site term. Overall, the all site term residuals seem to behave better than the Lg site term residuals, especially at higher frequencies. The site response models for the Sichuan Basin were derived using Fourier spectra, which can be used to develop site terms applicable for prediction models of the PSA response spectra following the procedure in Chapman and Guo, 2021.

Conclusion

The crustal quality factor and site response in the Sichuan Basin and the Songpan-Ganze terrane were estimated using more than 5,800 three-component broadband seismograms from 189 earthquakes occurring between January 2009 and October 2020. We obtained $Q(f) = 313f^{0.74}$ and $Q(f) = 568f^{0.338}$ for the Sichuan Basin and Songpan-Ganze terrane respectively, which is in good agreement with the $Q(f)$ models found in previous studies. Site responses of stations in the Sichuan Basin differed strongly from those in the Songpan-Ganze terrane, which is attributed to the different geological conditions between the two regions. The average site response in the basin shows stronger amplification effects at frequencies lower than 6 Hz and strong attenuation effects at higher frequencies (>10 Hz) relative to the Songpan-Ganze terrane. κ_0 estimates of stations in the basin are generally larger than those in the Songpan-Ganze terrane and the average κ_0 is ~1.6 times larger in the basin than the Songpan-Ganze terrane. Site response terms and κ_0 of stations in the Sichuan Basin were found to be correlated with sediment thickness. We developed site response models for the Sichuan Basin from site response terms obtained using Lg Fourier amplitudes, coda spectral ratios and H/V spectral

ratios. The site response models depend on the sediment thickness and were incorporated in the stochastic method of ground motion predictions for six recent earthquakes, to establish an independent means to test the derived models. The rock site term residuals for the earthquakes exhibit strong bias, and dependence on sediment thickness, exhibiting an underestimation of low-frequency ground motions and overestimation of high-frequency ground motions in the Sichuan Basin. This bias of ground motion prediction residuals is greatly reduced using the site response models derived here. Generally, the Lg results and the results using all site term coefficients presented in this study worked well in predicting ground motions for the six earthquakes used to independently test the models. The site response models defined by Eqs 9, 11 are the first models developed for the whole Sichuan Basin which can be directly used in predicting the Fourier spectra recorded at stations with given sediment thickness. Site corrections based on our site response models can be used to reduce the bias in determining magnitudes and other source parameters of the earthquakes in the Longmen Shan and adjacent regions. In addition, site terms for predicting PSA response spectra can be developed from our site response models following the method in Chapman and Guo 2021, which can be incorporated into calculations of probabilistic seismic hazard assessment. Soc,

Data and resources

The seismic data used in this study are provided by Data Management Centre of China National Seismic Network at Institute of Geophysics (SEISDMC, doi:10.11998/SeisDmc/SN), China Earthquake Networks Center and AH, BJ, BU, CQ, FJ, GD, GS, GX, GZ, HA, HB, HE, HI, HL, HN, JL, JS, JX, LN, NM, NX, QH, SC, SD, SH, SN, SX, TJ, XJ, XZ, YN, ZJ Seismic Networks, China Earthquake Administration (http://www.esdc.ac.cn/; last accessed June 2022). We made some of the figures using the Generic Mapping Tools version 5.2.1 (GMT, Wessel et al., 2013) and Matplotlib version 1.5.1 (Hunter, 2007).

Data availability statement

The original contributions presented in the study are included in the article/Supplementary Material, further inquiries can be directed to the corresponding author.

Author contributions

ZG: The first author collected and processed all the seismic data used in the study. She wrote the manuscript and plotted all the figures in the paper. MC: The corresponding author wrote and tested the fortran programs for the inversion and provided fortran programs for calculating the residuals. He described and explained some of the results during oral communications. He also revised the manuscript.

Funding

This study was supported by the National Natural Science Foundation of China (Grant No. 42004035), the Natural Science Foundation of Jiangsu Province (Grant No. BK20200609), and the Fundamental Research Funds for the Central Universities (Grant No. JUSRP121050).

Acknowledgments

We thank the Earthquake Science Data Center for providing the seismic data. We thank the associate editor YR and two reviewers for comments that improved the study.

Conflict of interest

The authors declare that the research was conducted in the absence of any commercial or financial relationships that could be construed as a potential conflict of interest.

Publisher's note

All claims expressed in this article are solely those of the authors and do not necessarily represent those of their affiliated organizations, or those of the publisher, the editors and the reviewers. Any product that may be evaluated in this article, or claim that may be made by its manufacturer, is not guaranteed or endorsed by the publisher.

Supplementary material

The Supplementary Material for this article can be found online at: https://www.frontiersin.org/articles/10.3389/feart.2022.1016096/full#supplementary-material

References

Anderson, J. G., and Hough, S. E. (1984). A model for the shape of the Fourier amplitude spectrum of acceleration at high frequencies. *Bull. Seismol. Soc. Am.* 74, 1969–1993.

AQSIQ (2001). *GB18306—2011 seismic ground motion parameters zonation map of China*. first edition. Beijing: Standard Press of China, 165–189. AvaliableAt: https://www.nssi.org.cn/nssi/front/5138636.html.

Atkinson, G. M., and Mereu, R. F. (1992). The shape of ground motion attenuation curves in southeastern Canada. *Bull. Seismol. Soc. Am.* 82 (5), 2014–2031. doi:10.1785/bssa0820052014

Atkinson, G. M., and Boore, D. M. (2014). The attenuation of Fourier amplitudes for rock sites in eastern North America. *Bull. Seismol. Soc. Am.* 104, 513–528. doi:10.1785/0120130136

Baqer, S., and Mitchell, B. (1998). Regional variation of. *Pure Appl. Geophys.* 153 (4), 613–638. doi:10.1007/s000240050210

Bora, S. S., Scherbaum, F., Kuehn, N., and Stafford, P. (2016). On the relationship between Fourier and response spectra: Implications for the adjustment of empirical ground-motion prediction equations (GMPEs). *Bull. Seismol. Soc. Am.* 106 (3), 1235–1253. doi:10.1785/0120150129

Borcherdt, R. D. (2002). Empirical evidence for acceleration-depen- dent amplification factors. *Bull. Seismol. Soc. Am.* 92, 761–782. doi:10.1785/0120010170

Boore, D. M., and Thompson, E. M. (2015). Revisions to some parameters used in stochastic-method simulations of ground motion. *Bull. Seismol. Soc. Am.* 105, 1029–1041. doi:10.1785/0120140281

Brune, J. N. (1971). Correction. *J. Geophys. Res.* 76, 5002.

Brune, J. N. (1970). Tectonic stress and the spectra of seismic shear waves from earthquakes. *J. Geophys. Res.* 75, 4997–5009. doi:10.1029/jb075i026p04997

Burchfiel, B. C., Chen, Z. L., Liu, Y. P., and Royden, L. H. (1995). Tectonics of the longmen Shan and adjacent regions, central China. *Int. Geol. Rev.* 37 (8), 661–735. doi:10.1080/00206819509465424

Burger, R. W., Somerville, P. G., Barker, J. S., Herrmann, R. B., and Helmberger, D. V. (1987). The effect of crustal structure on strong ground motion attenuation relations in eastern North America. *Bull. Seismol. Soc. Am.* 77, 420–439.

Campbell, K. W. (2009). Estimates of shear-wave Q and 0 for unconsolidated and semiconsolidated sediments in eastern north Americafor unconsolidated and semiconsolidated sediments in eastern north America. *Bull. Seismol. Soc. Am.* 99 (4), 2365–2392. doi:10.1785/0120080116

Castro, R. R., Stock, J. M., Hauksson, E., and Clayton, R. W. (2017). Source functions and path. Report.

Chang, E. Z. (2000). Geology and tectonics of the songpan-ganzi fold belt, southwestern China. *Int. Geol. Rev.* 42 (9), 813–831. doi:10.1080/00206810009465113

Chang, S. C., Wen, K. L., Huang, M. W., Kuo, C. H., Lin, C. M., Chen, C. T., and Huang, J. Y. (2019). The high-frequency decay parameter (Kappa) in Taiwan. *Pure Appl. Geophys.* 176, 4861–4879. doi:10.1007/s00024-019-02219-y

Chapman, M., and Conn, A. (2016). A model for Lg propagation in the Gulf Coastal Plain of the southern United States. *Bull. Seismol. Soc. Am.* 106 (2), 349–363. doi:10.1785/0120150197

Chapman, M., and Guo, Z. (2021). A response spectral ratio model to account for amplification and attenuation effects in the atlantic and Gulf Coastal Plain. *Bull. Seismol. Soc. Am.* 111 (4), 1849–1867. doi:10.1785/0120200322

Chen, X. B., Wu, Y. Q., Du, P. S., Li, J. S., Wu, Y. R., and Jiang, G. F. (1986). "Crustal velocity structure at two sides of Longmenshan tectonic belt (in Chinese)," in *Developments in the research of deep structure of China's continent* (Beijing: Seismol. Press), 112–127.

Field, E. H., Johnson, P. A., Beresnew, l. A., and Zeng, Y. (1997). Nonlinear ground-motion amplification by sediments during the 1994 Northridge earthquake. *Nature* 390 (11), 599–602. doi:10.1038/37586

Frankel, A. D., Carver, D. L., and Williams, R. A. (2002). Nonlinear and linear site response and basin effects in Seattle for the M 6.8 Nisqually, Washington, earthquake. *Bull. Seismol. Soc. Am.* 92 (6), 2090–2109. doi:10.1785/0120010254

Frankel, A. (1991). Mechanisms of seismic attenuation in the crust: Scattering and anelasticity in New York state, south Africa, and southern California. *J. Geophys. Res.* 96, 6269–6289. doi:10.1029/91jb00192

Fu, L., and Li, X. (2016). The characteristics of high-frequency attenuation of shear waves in the Longmen Shan and adjacent regions. *Bull. Seismol. Soc. Am.* 106 (5), 1979–1990. doi:10.1785/0120160002

Fu, L., Li, X., Wang, F., and Chen, S. (2019). A study of site response and regional attenuation in the Longmen Shan region, eastern Tibetan Plateau, SW China, from seismic recordings using the generalized inversion method. *J. Asian Earth Sci.* 181, 103887. doi:10.1016/j.jseaes.2019.103887

Fu, L., Li, X. J., Rong, M. S., Chen, S., and Zhou, Y. (2018). Parameter estimation of ground-motion prediction model in Longmen Shan region based on strong motion data. *Acta Seismol. Sin.* 40, 374–386. doi:10.11939/jass.20170215

Guo, Z., and Chapman, M. C. (2019). An examination of amplification and attenuation effects in the Atlantic and Gulf Coastal Plain using spectral ratios. *Bull. Seismol. Soc. Am.* 109 (5), 1855–1877. doi:10.1785/0120190071

Guo, Z., Guan, M., and Chapman, M. C. (2022). Amplification and attenuation due to geologic conditions in the Sichuan Basin, central China. *Seismol. Res. Lett.* XX, 1–15. doi:10.1785/0220220030

Guo, Z. W., Deng, K., and Han, Y. (1996). *Formation and evolution of the Sichuan Basin*. Beijing: Geologic Publishing House, 200.

Harmon, J., Hashash, Y. M. A., Stewart, J. P., Rathje, E. M., Campbell, K. W., and Silva, W. J. (2019). Site amplification functions for central and eastern North America—Part II: Modular simulation-based models. *Earthq. Spectra* 35 (2), 815–847. doi:10.1193/091117EQS179M

Hua, W., Chen, Z. L., and Zheng, S. H. (2009). A study on segmentation characteristics of aftershock source parameters of Wenchuan M8.0 earthquake in 2008. *Chin. J. Geophys.* 52, 365–371. doi:10.1002/cjg2.1334

Hunter, J. D. (2007). Matplotlib: A 2D graphics environment. *Comput. Sci. Eng.* 9 (3), 90–95. doi:10.1109/mcse.2007.55

Kennett, B. L. N. (1986). Lg waves and structural boundaries. *Bull. Seismol. Soc. Am.* 76, 1133–1141.

Kirby, E., Reiners, P. W., Krol, M. A., Whipple, K. X., Hodges, K. V., and Farley, K. A. (2002). Late Cenozoic evolution of the eastern margin of the Tibetan Plateau: Inferences from $^{40}Ar/^{39}Ar$ and (U-Th)/He thermochronology. *Tectonics* 21, 1–20. doi:10.1029/2000TC001246

Li, J., Zhou, B., Rong, M., Chen, S., and Zhou, Y. (2020). Estimation of source spectra, attenuation, and site responses from strong-motion data recorded in the 2019 changning earthquake sequence. *Bull. Seismol. Soc. Am.* 110 (2), 410–426. doi:10.1785/0120190207

Li, X., Zhai, C., Wen, W., and Xie, L. (2018a). Ground motion prediction model for horizontal PGA, 5% damped response spectrum in sichuan-yunnan region of China. *J. Earthq. Eng.* 24, 1829–1866. doi:10.1080/13632469.2018.1485600

Li, Y., He, D., Li, D., Lu, R., Fan, C., and Sun, Y. (2018b). Sedimentary provenance constraints on the jurassic to cretaceous paleogeography of Sichuan Basin, SW China. *Gondwana Res.* 60, 15–33. doi:10.1016/j.gr.2018.03.015

Li, Y. Q., He, D. F., Chen, L. B., Mei, Q. H., Li, C. X., and Zhang, L. (2016). Cretaceous sedimentary ba- sins in sichuan, SW China: Restoration of tectonic and depositional environments. *Cretac. Res.* 57, 50–65. doi:10.1016/j.cretres.2015.07.013

Li, Z. W., Xu, Y., Huang, R. Q., Hao, T. Y., Xu, Y., Liu, J. S., et al. (2011). Crustal P-wave velocity structure of the Longmen Shan region and its tectonic implications for the 2008 Wenchuan earthquake. *Sci. China Earth Sci.* 54, 1386–1393. doi:10.1007/s11430-011-4177-2

Liu, S., Yang, Y., Deng, B., Zhong, Y., Wen, L., Sun, W., et al. (2021). Tectonic evolution of the Sichuan Basin, southwest China. *Earth. Sci. Rev.* 213, 103470. doi:10.1016/j.earscirev.2020.103470

Liu, Z., Wuenscher, M. E., and Herrmann, R. B. (1994). Attenuation of body waves in the central New Madrid seismic zone. *Bull. Seismol. Soc. Am.* 84, 1112–1122.

Meng, Q. R., Wang, E. C., and Hu, J. M. (2005). Mesozoic sedimentary evolution of the northwest Sichuan basin: Implication for continued clockwise rotation of the South China block. *Geol. Soc. Am. Bull.* 117, 396–410. doi:10.1130/b25407.1

Ou, G. B., and Herrmann, R. B. (1990). A statistical model for ground motion produced by earthquakes at local and regional distances. *Bull. Seismol. Soc. Am.* 80 (6A), 1397–1417. doi:10.1785/bssa08006a1397

Pasyanos, M. E., Matzel, E. M., Walter, W. R., and Rodgers, A. J. (2009). Broad-band*Lg*attenuation modelling in the Middle East. *Geophys. J. Int.* 177, 1166–1176. doi:10.1111/j.1365-246x.2009.04128.x

Pratt, T. L., and Schleicher, L. S. (2021). Characterizing ground- motion amplification by extensive flat-lying sediments: The seismic response of the eastern U.S. Atlantic Coastal Plain strata. *Bull. Seismol. Soc. Am.* 111, 1795–1823. doi:10.1785/0120200328

Sha, J. G., Shi, X. Y., Zhou, Z. H., and Wang, Y. D. (2010). *The terrestrial triassic and jurassic sys- tems in the Sichuan Basin*. ChinaHefei: University of Science & Technology of China Press, 1–214.

Steidl, J. H., Tumarkin, A. G., and Archuleta, R. J. (1996). What is a reference site? *Bull. Seismol.* 86, 1733–1748.

Stewart, J. P., Parker, G. A., Atkinson, G. M., Boore, D. A., Hashash, Y. M. A., and Silva, W. J. (2020). Ergodic site amplification model for central and eastern North America. *Earthq. Spectra* 36 (1), 42–68. doi:10.1177/8755293019878185

Tian, Y., Kohn, B. P., Phillips, D., Hu, S., Gleadow, A. J. W., and Carter, A. (2016). Late Cretaceous–earliest Paleogene deformation in the Longmen Shan fold- and-thrust belt, eastern Tibetan Plateau margin: Pre-Cenozoic thickened crust? *Tectonics* 35, 2293–2312. doi:10.1002/2016TC004182

Wang, C.-Y., Han, W.-B., Wu, J.-P., Lou, H., and Chan, W. W. (2007). Crustal structure beneath the eastern margin of the Tibetan Plateau and its tectonic implications. *J. Geophys. Res.* 112, B07307. doi:10.1029/2005JB003873

Wang, H., Xie, L., Wang, S., and Ye, P. (2013). Site response in the Qionghai Basin in the wenchuan earthquake. *Earthq. Eng. Eng. Vib.* 12, 195–199. doi:10.1007/s11803-013-0162-4

Wang, H., Li, C., Wen, R., and Ren, Y. (2022). Integrating effects of source-dependent factors on sediment-depth scaling of additional site amplification to ground-motion prediction equation. *Bull. Seismol. Soc. Am.* 112 (1), 400–418. doi:10.1785/0120210134

Wang, H., Ren, Y., and Wen, R. (2018). Source parameters, path attenuation and site effects from strong-motion recordings of the Wenchuan aftershocks (2008-2013) using a non-parametric generalized inversion technique. *Geophys. J. Int.* 212, 872–890. doi:10.1093/gji/ggx447

Wang, H., and Wen, R. (2021). Attenuation and basin amplification revealed by the dense ground motions of the 12 July 2020 MS 5.1 Tangshan, China, earthquake. *Seismol. Res. Lett.* 94 (2), 2109–2121. doi:10.1785/0220200400

Wang, M. M., Hubbard, J., Plesch, A., Shaw, J. H., and Wang, L. N. (2016). Three-dimensional seismic velocity structure in the Sichuan basin, China. *J. Geophys. Res. Solid Earth* 121 (2), 1007–1022. doi:10.1002/2015jb012644

Wei, Z., Chu, R., Chen, L., Wu, S., Jiang, H., and He, B. (2020). The structure of the sedimentary cover and crystalline crust in the Sichuan Basin and its tectonic implications. *Geophys. J. Int.* 223 (3), 1879–1887. doi:10.1093/gji/ggaa420

Wen, R., Ren, Y., Zhou, Z., and Shi, D. (2010). Preliminary site classification of free-field strong motion stations based on Wenchuan earthquake records. *Earthq. Sci.* 23, 101–110. doi:10.1007/s11589-009-0048-8

Wessel, P., Smith, W. H. F., Scharroo, R., Luis, J. F., and Wobbe, F. (2013). Generic mapping Tools: Improved version released. *Eos Trans. AGU.* 94, 409–410. doi:10.1002/2013eo450001

Wu, W. W., Su, J. R., Wei, Y. L., Wu, P., Li, J., and Sun, W. (2016). Discussion on attenuation characteristics, site response and magnitude determination in Sichuan. *Seimol. Geol.* 38, 1005–1018. doi:10.3969/j.issn.0253-4967.2016.04016

Xia, X., Li, Z., Bao, F., Xie, J., Shi, Y., You, Q., et al. (2021). Sedimentary structure of the Sichuan Basin derived from seismic ambient noise tomography. *Geophys. J. Int.* 225, 54–67. doi:10.1093/gji/ggaa578

Xie, J., Wu, Z., Liu, R., Schaff, D., Liu, Y., and Liang, J. (2006). Tomographic regionalization of crustal Lg Q in eastern Eurasia. *Geophys. Res. Lett.* 33, L03315. doi:10.1029/2005GL024410

Xu, P., Ren, Y., Wen, N., and Wang, H. (2020). Observations on regional variability in ground-motion amplitude from six mw ~ 6.0 earthquakes of the north–south seismic zone in China. *Pure Appl. Geophys.* 177, 247–264. doi:10.1007/s00024-019-02176-6

Zhao, L.-F., Xie, X.-B., Wang, W.-M., Zhang, J.-H., and Yao, Z.-X. (2010). Seismic Lg-wave Q tomography in and around Northeast China. *J. Geophys. Res.* 115, B08307. doi:10.1029/2009JB007157

Zheng, C., Zhang, R., Wu, Q., Li, Y., Zhang, F., Shi, K., et al. (2019). Variations in crustal and uppermost mantle structures across eastern Tibet and adjacent regions: Implications of crustal flow and asthenospheric upwelling combined for expansions of the Tibetan plateau. *Tectonics* 38, 3167–3181. doi:10.1029/2018TC005276

Zheng, Y., Li, H., Sun, Z., Wang, H., Zhang, J., Li, C., et al. (2016). New geochronology constraints on timing and depth of the ancient earthquakes along the Longmen Shan fault belt, eastern Tibet. *Tectonics* 35, 2781–2806. doi:10.1002/2016TC004210